JOURNAL OF PROPULSION AND POWER
Vol. 14, No. 6, November–December 1998

Numerical Prediction of Unsteady Transitional Boundary Layer Caused by Rotor–Stator Interaction

Dongjin Kang* and Budugur Lakshminarayana†
Pennsylvania State University, University Park, Pennsylvania 16802

The objective of the research reported in this paper was to develop computational techniques for the prediction of transitional flows associated with the rotor–stator interaction in turbomachinery. Three low-Reynolds-number turbulence models were incorporated in the Navier–Stokes code and evaluated for accuracy in predicting the onset and end of unsteady transitional patches caused by wake passing. The best model was then used for the modification and improvement of the leading-edge effect. A comparison with the experimental data indicated that the quality of prediction was as good as those derived from an unsteady boundary-layer code. A comparison of the instantaneous shape factor, the skin friction coefficient, and the momentum thickness indicated that the Navier–Stokes predictions were reasonably good and should aid the designers of turbomachinery in allowing for the unsteady transitional flows caused by rotor–stator interaction. The simulation results were interpreted to derive new insight on the flow physics associated with transitional flow including turbulence properties.

Nomenclature

C = chord length
C_f = skin friction coefficient $2\tau_w/\rho V_\infty^2$
C_p = unsteady pressure coefficient $(p - \bar{p})/\frac{1}{2}\rho V_\infty^2$
H = shape factor δ^*/θ
k = turbulent kinetic energy
p = static pressure
ps = pressure surface
R = Reynolds number, $(\rho V_\infty C)/\mu$
R_y = $\sqrt{k}y/\nu$
R_θ = momentum Reynolds number $(\rho V_\infty \theta)/\mu$
ss = suction surface
ssc = distance from the leading edge along the suction surface
ssl = suction surface length
T = wake pasing period
t = time
U_m = rotor speed at midspan
u, v = streamwise (x) and normal (y) velocity component
u', v' = unsteady velocity components, $u - \bar{u}$, $v - \bar{v}$, respectively
V = total velocity
V_e = velocity at boundary-layer edge
V_{trailing} = boundary-layer edge velocity at the trailing edge
x_i = Cartesian coordinates
y = distance from the surface
y^+ = dimensionless distance from the wall, $\rho y u_\tau/\mu$
δ^* = displacement thickness
θ = momentum thickness
μ, μ_t = molecular and turbulent eddy viscosity
ρ = density
$\overline{\rho u_i u_j}$ = Reynolds stress tensor
τ_{ij} = stress tensor
φ = phase angle of a harmonic
ω_r = reduced frequency $\omega C/U_m$

Subscripts
e = edge value
w = wall
∞ = upstream values

Superscript
$-$ = time-averaged quantities

Presented as Paper 97-2752 at the AIAA/ASME/SAE/ASEE 33rd Joint Propulsion Conference, Seattle, WA, July 6–9, 1997; received Aug. 30, 1997; revision received May 18, 1998; accepted for publication May 19, 1998.

*Visiting Assistant Professor of Aerospace Engineering on sabbatical leave from Yeungnam University, School of Mechanical Engineering, Gyongsan, South Korea.

†Evan Pugh Professor of Aerospace Engineering and Director, Center for Gas Turbines and Power, 153 Hammond Building. Fellow AIAA.

Introduction

ONE of the most challenging problems in turbomachinery is to understand the unsteady flow physics associated with the rotor–stator interaction, particularly the transitional boundary layer along the blade surfaces. Such complex unsteady and transitional boundary-layer flow is known to affect the aerodynamic, structural, and thermal performance of a turbomachine. Considerable attention has been paid in recent years in developing computer codes to predict unsteady aerodynamics and heat transfer, but these efforts are hampered by a lack of understanding of the physical modeling (transition/turbulence models) and validation of the codes. A computational code with artificial dissipation and numerical error may mask some of the important physics. The code must be validated at several stages to ensure that the flow physics are captured accurately. Even the steady flow prediction with higher-order turbulence models is not satisfactory because of the inadequacy of physical models employed. There is a need to assess these numerical techniques and improve the computational efficiency. There has been a very limited computational effort to resolve the flow physics and provide an accurate prediction of the unsteady transitional viscous layers. Fan and Lakshminarayana[1] used a Euler/boundary-layer approach and modified the turbulence models to predict the unsteady transitional viscous layers in compressors and turbines, for which detailed data are available.[2,3]

No attempts have been made to assess the capability of the Navier–Stokes code to predict the unsteady transitional viscous layers caused by wake–blade interaction. This is the objective of the research reported in this paper. The Euler/boundary layer procedure developed by Fan and Lakshminarayana is very efficient because of the parabolic nature of the viscous

layers. But this procedure is restricted to thin unseparated viscous layers, and its accuracy depends on the accuracy of the Euler solution. The Navier–Stokes code, on the other hand, is more general and does not depend on an inviscid/viscid uncoupled procedure. Its disadvantage is in high CPU time as a result of a large number of grids (typically first grid point, $y^+ = 1$) required for the computation of the amplitude and the phase angle of various flow properties inside the viscous layers.

A systematic approach is undertaken in the paper to assess the ability of the Navier–Stokes code to predict the unsteady transitional boundary layer. An existing code is assessed for grid sensitivity and time step. Various turbulence models are assessed for accuracy in predicting the transitional boundary layers. After the calibration stages, the code is validated against the compressor data by Halstead et al.[3] Furthermore, the simulation data are used to extract information on the flow physics.

Navier–Stokes Procedure

Two approaches are pursued in this paper. The first approach is the Euler/boundary-layer procedure from Fan and Lakshminarayana. The second approach is the Navier–Stokes procedure developed in this paper. The Navier–Stokes procedure, which is the main emphasis of this paper, is described in this section followed by a brief overview of the Euler/boundary-layer procedure.

The Reynolds-averaged Navier–Stokes equations for two-dimensional unsteady incompressible flow are solved. To simulate transitional boundary-layer flow along the blade, three different low-Reynolds-number k-ε turbulence models are used. The turbulence models considered here are those of Chien's model (C),[4] Lam and Bremhost (L–B),[5] and Fan, Lakshminarayana, and Barnett's model (F–L–B).[6] The turbulent viscosity is represented as

$$\mu_t = \rho c_\mu f_\mu (k^2/\tilde{\varepsilon}), \qquad \varepsilon = \tilde{\varepsilon} + D \tag{1}$$

where $\tilde{\varepsilon}$ is a modified dissipation rate from the turbulent kinetic energy dissipation rate ε, c_μ is a model constant, and f_μ is a model function. The function D is used in some turbulent models to get a Dirichlet boundary condition $\tilde{\varepsilon} = 0$ for $\tilde{\varepsilon}$.

Three low-Reynolds-number turbulence models chosen in this research were developed in a similar way, but differ in the treatment of wall damping and/or a low-Reynolds-number effect near the wall. Chien's model[4] uses the viscous sublayer y^+ to simulate a low-Reynolds-number effect, whereas the L–B model[5] uses a turbulent Reynolds number defined as $R_t = k^2/\nu\varepsilon$. The F–L–B model[6] is the most delicate one in the sense that it attempts to separate the wall damping effect from the low-Reynolds-number effect. The F–L–B model uses a new function given by

$$f_w = 1 - \exp\left\{-\frac{\sqrt{R_y}}{2.30} + \left(\frac{\sqrt{R_y}}{2.30} - \frac{R_y}{8.89}\right)\left[1 - \exp\left(-\frac{R_y}{20}\right)\right]^3\right\} \tag{2}$$

There have been several attempts to develop transition models that could be incorporated into a turbulence model. Recent attempts are from Chakka and Schobeiri.[7] The objective of the present paper, however, is to attempt the prediction directly from the low-Reynolds-number k-ε model. Most low-Reynolds-number turbulence models mimic the structure of a turbulent boundary layer (viscous sublayer, buffer layer, and law of the wall region), and this structure is quite similar to the progressive stages experienced by a transitional boundary layer. Thus, the transition process could be naturally simulated by using a low-Reynolds-number k-ε model.[1] Some investigators employ the algebraic eddy viscosity model and specify the location of transition onset and end of transition using the correlation by Abu-Ghannam and Shaw[8] This correlation is based on the momentum Reynolds number and freestream turbulence intensity. According to Savill,[9] the low-Reynolds-number turbulence models, which simulate the wall damping effect with a variable such as R_t, perform better than others with $R_y = \sqrt{k}y/\nu$ or y^+. Thus, of the three turbulence models chosen in this paper, the L–B and F–L–B models are expected to perform better. In addition, the F–L–B model has been validated for unsteady boundary-layer flows.[6]

Time-accurate solutions are obtained by using the second-order-backward Euler scheme for the time derivatives, whereas the second-order spatial accuracy is preserved by using the central difference scheme for diffusion terms and the QUICK scheme for convection terms. The governing equations are transformed to a generalized nonorthogonal coordinate system. Details of the numerical scheme are given in Ho and Lakshminarayana.[10] The artificial dissipation terms, which play a crucial role in convergence and accuracy, are not used in this study.

The experimental values of time-dependent velocity profiles are specified as inlet boundary conditions, and the no-slip condition is enforced along the blade surfaces. The velocity at the exit boundary is calculated by solving the governing equations. For the pressure equation, the normal derivative of pressure is assumed to be zero at inlet and exit boundaries, as well as on the blade surfaces. As the Neumann type of boundary condition for the pressure equation is used, the pressure needs to be specified at least at one grid point to ensure convergence. The pressure is specified at the midpoint of the exit boundary.

Code Validation and Simulation

It is necessary to validate the Navier–Stokes code and study the grid sensitivity, the effect of time step size, and the effects of artificial dissipation. A detailed study was undertaken to assess the optimum step size, which depends on the time scale of the fluctuating flowfield and the grid size. The experimental data obtained by Stauter et al.[11] was chosen as a test case for the validation of the present code and to investigate the effects of time step size for a wake passing period on unsteady flow characteristics. The case chosen here is the unsteady flowfield through the second-stage stator of a multistage compressor investigated at United Technologies Research Center (UTRC). The UTRC multistage compressor is operated at a flow coefficient of 0.51 and at a Reynolds number of 2.5×10^5, based on the blade chord length, and is operated at the reduced frequency $\omega_r = 8.48$.

The inlet computational domain is at 36% of the axial chord upstream of the second-stage stator. This corresponds to one of Stauter et al.'s[11] measurement stations. The measured velocity profile (wake) is used as an input, and the exit boundary extends to 85% of the axial chord downstream of the stator. The computational grid consists of 200×96 grid points downstream. The turbulence intensity at the inlet boundary is specified as 9%. Three differing time steps are attempted, and these are 300, 600, and 1000 for a wake passing period. The time-averaged blade pressure distribution (not shown) on the stator blade agrees very well with the earlier computations by Gundy-Burlet et al.[12] The magnitude and phase angle of the first five harmonics of unsteady velocity fluctuations near the leading edge are independent of the time step size. However, the deviation in the distribution of C_p with the time step size is found to be larger than those in the velocity profiles. Because the pressure has a dimension of $[\rho V^2]$, the fluctuation in velocity corresponds to a larger value in the fluctuation of pressure. However, the third harmonic of the suction surface pressure fluctuation with 300 time steps shows about 20% deviation from the 600 time steps solution at 20% of the axial chord. Therefore, 600 time steps per wake passing period are used in the following simulation.

Euler/Boundary-Layer Procedure

A compressible two-dimensional Euler equation was used in combination with an unsteady boundary-layer code to predict the unsteady transitional boundary-layer caused by rotor–stator interaction. The procedure is described in detail by Fan and Lakshminarayana.[1] Only a brief summary is given here. The standard four-stage Runge–Kutta scheme is used to integrate the equations. Central differences are used to discretize the spatial derivatives. Fourth-order artificial dissipation is used to stabilize the Runge–Kutta scheme.[13] Periodic boundary conditions are used in the pitchwise direction as in a steady solution. The coding technique in the present program allows for the solution to be carried out for an arbitrary number of blade passages. At the inlet and outlet boundaries, three-dimensional nonreflecting boundary conditions are used. Nonreflecting boundary conditions have been implemented in this code.

The unsteady two-dimensional compressible boundary-layer procedure and the code were originally developed by Power et al.,[14] using a mixing length turbulence model. A low-Reynolds-number form k-ε model (F–L–B model) was developed and implemented in this code by Fan et al.[6] A fully implicit numerical scheme is used to solve the transformed equations. The freestream turbulence is determined by solving the k-ε (simplified) equations at the outer edge of the solution domain using the velocities predicted from the Euler equations.

The temporal history of the freestream turbulence quantities (statistical properties) at the first streamwise station can be deduced from experimental measurements or Navier–Stokes solutions of the flow in the preceding blade row using a k-ε model. The code has been fully validated for various transitional boundary layers.[1]

Test Case

The General Electric research group[3] conducted a comprehensive experiment in their Low Speed Research Compressor (LSRC), and acquired data on the unsteady transitional boundary-layer development in a multistage environment. The LSRC is a three-stage compressor with inlet and outlet guide vanes. The relevant parameters are listed in Table 1. Detailed data were acquired on the surfaces of the third-stage rotor and stator. The instantaneous mean velocity and turbulence characteristics were acquired from a hot-wire survey at the exit of rotor 3.

A large number of hot-film sensors were mounted on the blade surface at the midspan region of stator 3, and this provided an accurate time history of periodic and random unsteadiness of skin friction stress and other relevant properties to assess the nature of unsteady transitional, calmed, and turbulent regions caused by the passage of the rotor 3 wake through the stator 3 passage at midspan. In addition, a hot-wire survey was conducted at midspan of the stator 3 to study the nature of unsteady transitional boundary layers at various chordwise locations. The present code is validated against data before carrying out additional simulation to understand the flow physics of unsteady transitional layer caused by the rotor–stator interaction.

Table 1 Compressor blading parameters[a]

	IGV	Rotor	Stator
Solidity	1.00	1.11	1.32
Aspect ratio	1.36	1.25	1.44
Chord, mm	83.8	91.2	79.1
Stagger, deg (axial)	19.6	46.9	13.9
Camber, deg	3.00	22.0	44.4
Number of airfoils	53	54	74
Axial gap, mm	98.0	25.4	——
Speed (design)	840 rpm	——	——
Flow coefficient	0.576	——	——
Pressure coefficient	0.74	——	——
Reynolds number (based on chord)			
Rotor 3	4.24×10^5	——	——
Stator 3	3.47×10^5	——	——

[a]Midspan.

The design point operation at the flow coefficient of 0.576 is considered (Table 1). The inlet boundary for the present computation is 16.5% upstream of the stator, and the outlet boundary is set at 100% downstream of the stator trailing edge. Because the position of the inlet boundary is one of the measurement stations, the experimental data are used as inlet boundary conditions for both the velocity components and the turbulence intensity. The computational grid consists of 252 × 202 grid points, with 150 grid points in the blade passage. Because the unsteady transitional boundary-layer flow depends on the turbulence models, three low-Reynolds-number k-ε turbulence models are used in the numerical simulation. The number of time steps per wake passing period is chosen as 600.

Modifications to the Turbulence Model

Preliminary computations were carried out with a coarse grid of 231 × 101 to assess the capability of turbulence models to capture the unsteady transitional boundary layer. Figure 1 shows space–time diagrams of shape factor derived from these

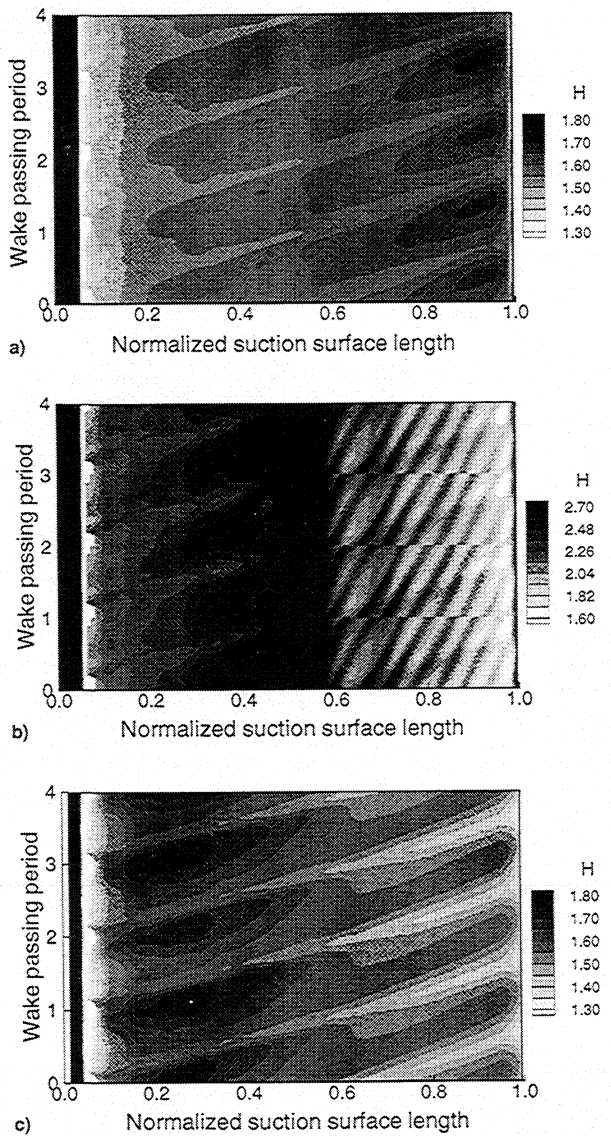

Fig. 1 Comparison of various turbulence models for transitional flow on the stator: a) Chien,[4] b) Lam and Brehost,[5] and c) Fan and Lakshminarayana[6] models.

three turbulence models after five periods. The computation with the L–B turbulence model is unstable and predicts much delayed transition, which leads to laminar separation at about 60% of the axial chord, resulting in numerical instability as evident from the figure. Even the computation with Chien's[4] model shows a relatively good convergence, but the solution is very poor compared with experimental data. The most prominent feature is the formation of the so-called "wake-induced transitional strip." A laminar boundary layer forms near the leading edge. The laminar boundary layer eventually undergoes transition to a turbulent boundary layer. The wake-induced transition strip is the loci of this transition region in the domain of space and time. However, Chien's solution doesn't capture this feature. F–L–B solution (Fig. 1c) seems to be the best one in terms of numerical stability and the capability of capturing the wake-induced strip. Even though the flow near the leading edge is fully turbulent, the characteristics of the wake-induced transition are captured well.

The formation of turbulent flow near the leading edge is inherent in all of the models used in this study (Fig. 1), and is a result of the inappropriateness of eddy viscosity models near the leading-edge region. Launder[15] pointed out that the conventional eddy viscosity models predict excessive turbulence levels near the stagnation point because of the nature of the constitutive stress-strain relation used in these turbulence models. Excessive production of the turbulent kinetic energy upstream of the leading edge results in a turbulent boundary layer in this region.

Two different types of modifications are suggested to overcome excessive generation of turbulent kinetic energy upstream of the leading edge. One of the suggestions is to change the turbulence model constants to balance the production term with the dissipation term.[16] The other and more popular suggestion is to modify the production term in the transport equation for the turbulent kinetic energy. For example, Launder[15] suggested the replacement of the turbulence energy generation term with the term

$$c_\mu \frac{k^2}{2\varepsilon} \sqrt{\left(\frac{\partial u_i}{\partial x_j} + \frac{\partial u_j}{\partial x_i}\right)^2 \left(\frac{\partial u_i}{\partial x_j} - \frac{\partial u_j}{\partial x_i}\right)^2}$$

This modification introduces the following vorticity parameter Ω instead of the mean shear rates:

$$\Omega = \frac{k}{\varepsilon} \sqrt{\frac{1}{2}\left(\frac{\partial u_i}{\partial x_j} - \frac{\partial u_j}{\partial x_i}\right)^2}$$

$$S = \frac{k}{\varepsilon} \sqrt{\frac{1}{2}\left(\frac{\partial u_i}{\partial x_j} + \frac{\partial u_j}{\partial x_i}\right)^2}$$

in the kinetic energy transport equation.

Results and Discussion

In the present study, the two modifications described in the previous section have been tried and Launder's modification was found to show improved predictions. Thus, the final computation of the unsteady transitional layer caused by the rotor/stator interaction is carried out with the F–L–B turbulence model, incorporating Launder's modification, with a grid size of 252 × 202, and 600 time steps per wake passing period. No such modification is done for the boundary-layer code because viscous flow computation with the k-ε model starts downstream of the leading edge. The grid size used for the Euler computation is 132 × 65 and the boundary layer employs 141 × 98 in the streamwise and normal directions, respectively.

The boundary-layer edge velocity predicted by the Navier–Stokes equation (normalized by velocity at the trailing edge) is shown compared with the experimental data in Fig. 2. The Navier–Stokes code predictions are in excellent agreement with the measured data. The maximum and minimum instantaneous velocities are also shown in this figure, but no such experimental data are available for comparison. The maximum unsteadiness occurs near the leading edge and this is consistent with prior investigations.

The time-averaged boundary-layer parameters (momentum Reynolds number and shape factor) are shown compared with the experimental data in Fig. 3. In addition, the computation from steady codes are reproduced from the paper by Halstead et al.[3] The boundary-layer solution from STANX is obtained by specifying the location of transition onset using Abu-Ghannam and Shaw's[8] correlation. The location of the onset of transition is determined from the transition correlation using the laminar mode of solution from STANX up to the onset of transition. The KEP code is a steady boundary-layer code with a low-Reynolds-number k-ε model.[17] The transition is simulated directly in this code. In the steady Navier–Stokes code an algebraic eddy viscosity model is used and the transition

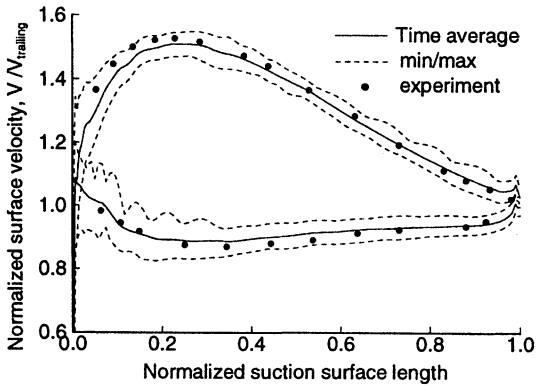

Fig. 2 Prediction of normalized surface velocity on stator blade.

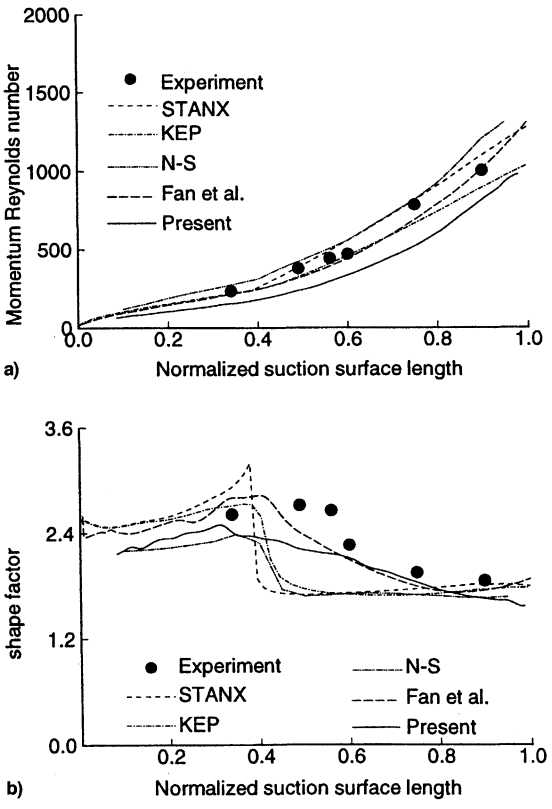

Fig. 3 Comparison between predicted momentum Reynolds number and measured time-averaged shape factor.

location is specified.[18] It should be emphasized here that the results from the unsteady codes are compared with these two steady codes (KEP and NS) to assess the quality of transition prediction. Both the steady (KEP) and unsteady boundary-layer codes show good agreement with the data for R_θ. The Navier–Stokes solution is less satisfactory, particularly near the trailing edge. The boundary-layer code employs three times as many grid points as the Navier–Stokes code because of the limitations of the computer. In any case, it is essential to resolve the pressure and velocity fields accurately, and the Navier–Stokes code is ideally suited for this purpose. The unsteady boundary-layer code and the unsteady Navier–Stokes code show much better agreement with the data on the shape factor than either of the steady codes. The transition is sudden in both of the steady codes. The inception of transition as well as the shape factor in the transitional zone is predicted well by the unsteady Euler/boundary-layer procedure and the Navier–Stokes code, even though the former provides a slightly better prediction. This is one of the critical tests for the unsteady flow solver to assess its ability to predict profile losses in blading with unsteady transitional layer.

The wake-induced unsteady transition can be clearly seen in the distribution of the shape factor along the suction surface in the space-time domain as shown in Fig. 4 and the momentum Reynolds number in Fig. 5. It should be remarked here that the k-ε model is employed downstream of the leading edge in the boundary-layer code, whereas the Navier–Stokes computation is based on the specification of turbulence intensity at the upstream computational plane. This is reflected in the turbulent patches near the leading edge for the Navier–Stokes computation (Fig. 5). The Navier–Stokes and Euler/boundary-layer solutions clearly capture the wake-induced transitional strip. However, the Euler/boundary layer solution shows the most delayed transition along the wake-induced transition strip, starting from about 40% of *ssl*, compared with 30% from the present solution and about 20% from the experimental data, estimated from Abu-Ghannam and Shaw's[8] correlation. Between the two consecutive wake trajectories, we can see the calmed region of laminar flow in all figures. The Navier–Stokes solution shows a less stable laminar region. This may be a result of several reasons, none of which can be confirmed because of the lack of experimental data.

1) The boundary-layer solution is based on the prescribed (from Euler code) pressure distribution in the freestream, whereas the Navier–Stokes code computes the pressure and velocity fields. The grid resolution may be one of the inadequacies of the latter.

2) Resolution of the pressure from the Navier–Stokes code near the leading and trailing edges is always a problem because

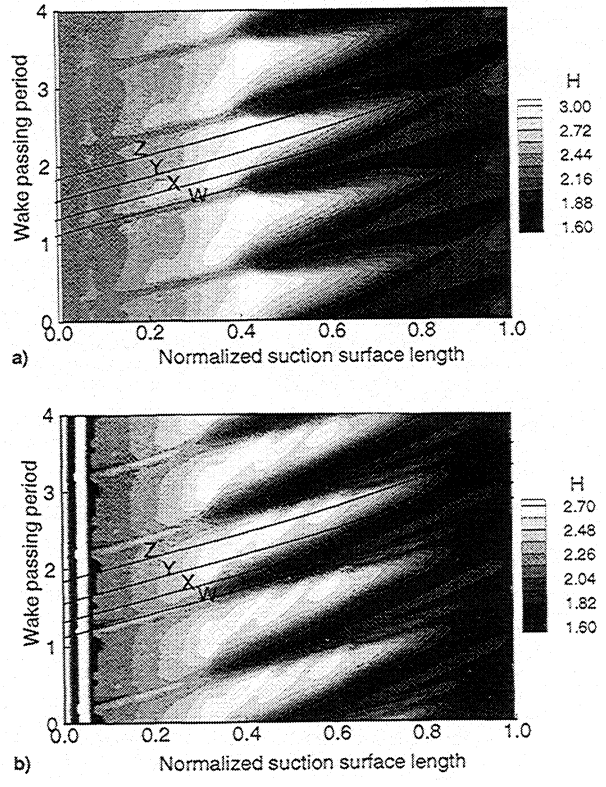

Fig. 4 Predicted distribution of instantaneous shape factor from a) Euler/boundary-layer and b) present Navier–Stokes solutions.

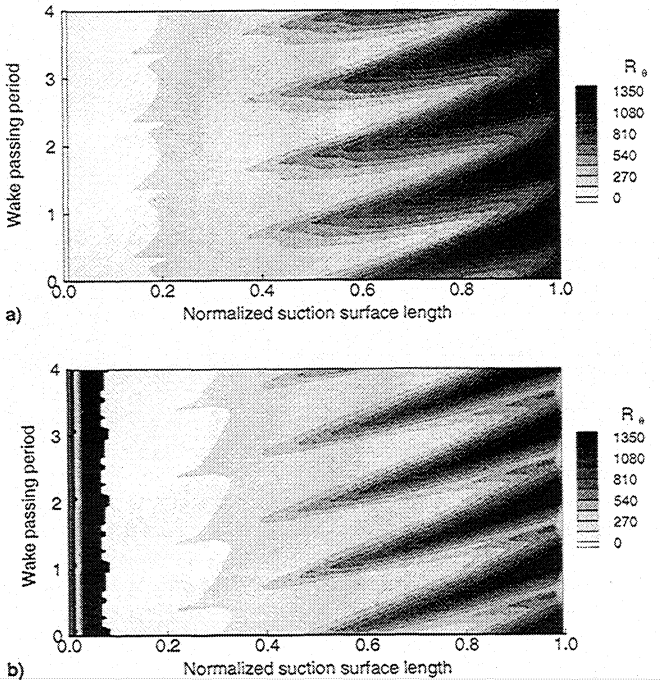

Fig. 5 Predicted distribution of instantaneous momentum Reynolds number: a) Euler boundary-layer and b) present Navier–Stokes solutions.

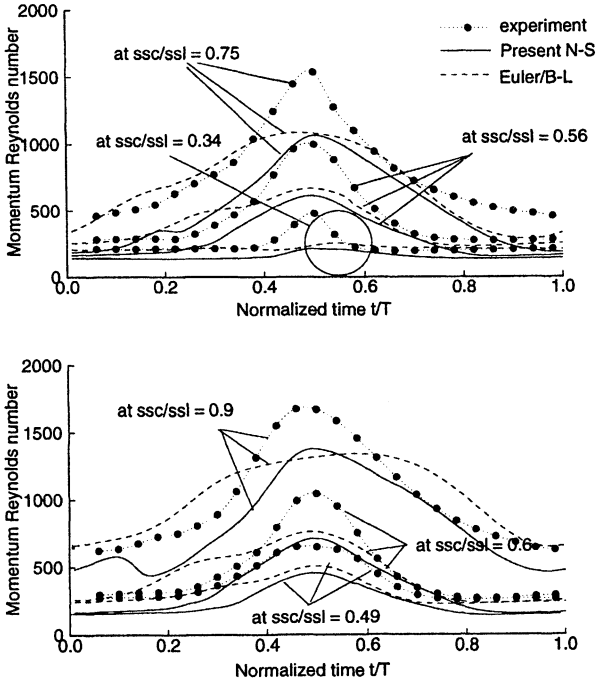

Fig. 6 Predicted and measured distribution of momentum Reynolds number at various chordwise locations.

of grid stretching and large velocity and pressure gradients in the region.

3) The phase lag between the pressure and velocity fluctuations in the freestream and the boundary layer may be one of the causes of the less stable laminar boundary layer. The Euler/boundary-layer procedure does not allow for a phase change in the pressure between the freestream and the boundary layer. The low turbulence intensity between two consecutive wake trajectories is directly imposed on the boundary layer, and this gives rise to a stable laminar flow.

4) The k-ε models do not perform well near the stagnation regions. This problem does not exist in the Euler/boundary-layer procedure. The transition ends at about 80% of *ssl* in the Euler/boundary-layer solution; again the shortest region. Along the wake trajectories, the momentum Reynolds number shows a strip of higher values, and this confirms relatively earlier transition along the wake.

The predicted time history of the momentum thickness is plotted in Fig. 5 and is shown compared with the available experimental data in Fig. 6. Both the Euler/boundary-layer and the Navier–Stokes code predict very similar momentum thickness distribution: even though the Euler/boundary-layer code predicts wider patches as can be seen in Fig. 6. Near the trailing edge (Fig. 6, *ssc/ssl* = 0.75 and 0.9), the Navier–Stokes code predicts a smaller magnitude of θ than the measured value, but the shape (time history) is almost identical to the measured distribution. On the other hand, the prediction from the Euler/boundary-layer procedure is in better agreement with the magnitude of θ, but the distribution is much flatter near the wake path. The phase lag in the pressure fluctuations between the freestream and the boundary-layer flow may be one of the causes of this discrepancy. The Euler/boundary-layer

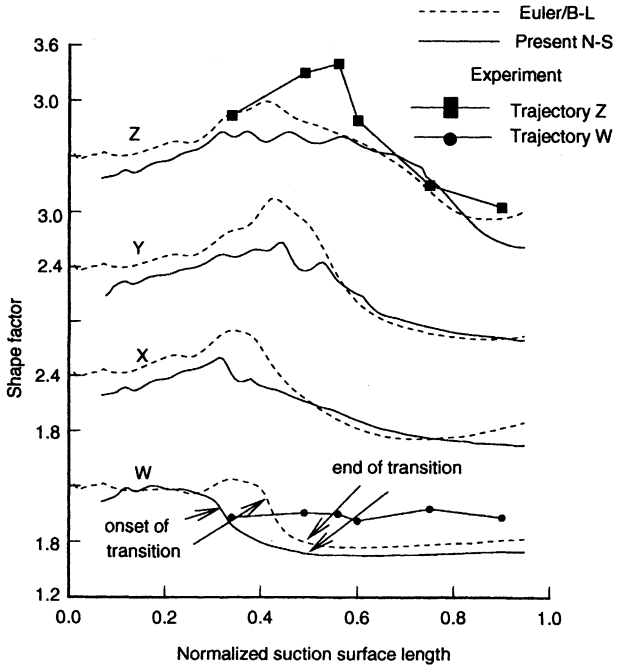

Fig. 7 Comparison between measured and predicted H along various trajectories shown in Fig. 4.

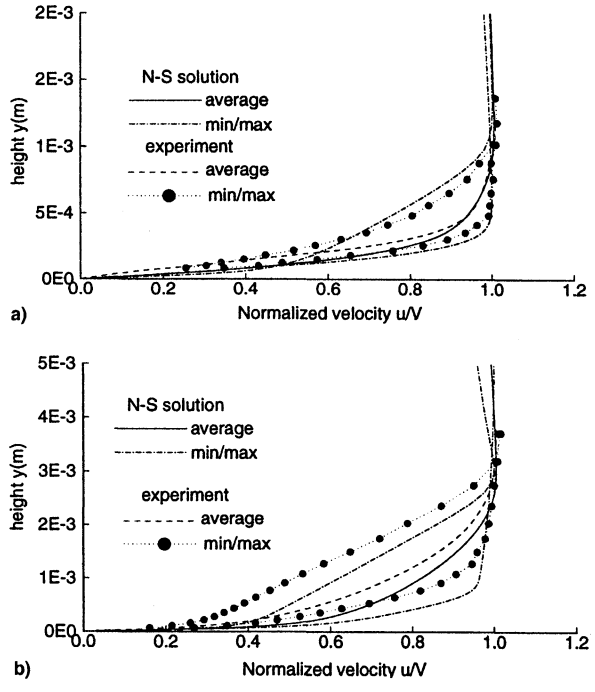

Fig. 8 Maximum, minimum, and average velocity profiles at 49 and 90% chord. *ssc/ssl* = a) 0.49 and b) 0.90.

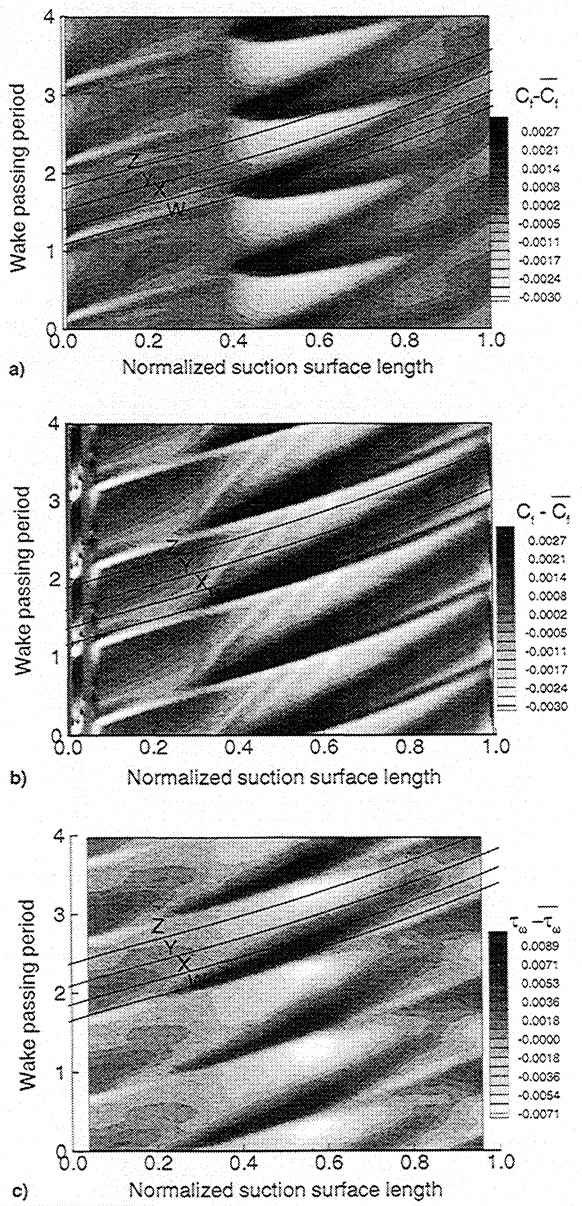

Fig. 9 Time history of measured and predicted fluctuations in skin friction coefficient: a) Euler boundary-layer solution, b) present Navier–Stokes solution, and c) experiment.

procedure assumes that the freestream pressure fluctuations are imposed inside the boundary layer and does not allow for any phase changes within the boundary layer.

Four trajectories labeled W, X, Y, and Z are drawn at a speed of $0.7V_\infty$, which is an average speed of the leading and trailing edge of the turbulent spot (Fig. 4). The trajectory W is drawn through the wake-induced transitional strip, and trajectories X, Y, and Z are located in time at 20, 44, and 72%, respectively, of the wake passing period behind the trajectory W. The distributions of the shape factor along these four trajectories are shown and compared with those from the boundary-layer computation in Fig. 7. The Euler/boundary-layer computation predicts the transition region at about 40–52% of *ssl* along the trajectory W, whereas the Navier–Stokes solution shows the transition to occur from about 30% of *ssl* and its length is about twice as long. Even the experimental data show no clear symptoms of transition in the shape-factor distribution. Halstead et al.[3] state that the onset of transition occurs at about 19% of *ssl* and its length is about 43% of *ssl*. As trajectories Y and Z lie midway between two consecutive upstream rotor wake trajectories, they show how the calmed region of the laminar boundary layer is formed. It should be remarked here that the boundary layers are very thin near the midchord (1–2 mm), and experimental uncertainties as well as numerical error contribute to the discrepancies observed between the data and predictions, particularly from 40–60% chord. The shape factor is very sensitive to the accuracy of the near-wall profiles. In addition, the actual flow is three dimensional, and the spanwise disturbances (three-dimensional effects) may cause earlier transition than the two-dimensional computations.

The velocity profiles at two typical locations are compared with the data in Fig. 8. Considering that the thickness of the boundary layer measured in the experiment is very thin (0.5–3 mm), the present solutions show good agreement with the experiment. The min/max profiles show that the unsteadiness caused by the relative motion of the upstream wake is captured reasonably well.

The wake-induced transitional strip is clearly seen in the time–space diagram of unsteady skin friction stress ($C_f - \bar{C}_f$) that is shown in Fig. 9. The wake-induced transitional strip predicted by the Euler/boundary-layer procedure is much shorter than those predicted by the Navier–Stokes code and the measured value. But the calmed region (lower strip–lighter color) is predicted better by the Euler/boundary-layer procedure. The Navier–Stokes solution shows scattering (less stable laminar flow) in this region. These results are consistent with the shape factor distribution shown in Fig. 4.

The transitional strip can be clearly seen in the turbulent kinetic energy distribution at four different locations normal to the wall plotted in Fig. 10. The lateral extensions of these strips are shown for one period at *ssc*/*ssl* = 0.3, 0.5, 0.7, and 0.9 in Fig. 11. The location of the wake trajectory (W) is also shown in these figures. These turbulent patches clearly confirm some of the conclusions drawn with regard to turbulent, transitional, and calm regions; as well as lateral spreading of the upstream wake and its effect. High turbulent intensity patches are located very close to the wall and are indicative of the upstream wake location as well as the interaction of counter-rotating vortices on either side of the moving wake. The turbulent patches extend across the entire period near the trailing edge. Maximum turbulence intensity occurs along the wake trajectory.

Very close correlation between the instantaneous momentum thickness (Figs. 5 and 7) and the turbulence intensity profile (Figs. 10 and 11) should be noted. Very interesting physical insight into the transitional flow can be derived by correlating the turbulent kinetic energy contours (Figs. 10 and 11), with the skin friction coefficient (Fig. 9), momentum thickness (Fig. 5), and shape-factor contours (Fig. 4). A small turbulent spot because of the wake appears near the 30% chord (Fig. 11), away from the wall. This indicates the beginning stages of inception of transition confirmed by the skin friction coefficient (Fig. 9) and the shape factor (Fig. 4). The upstream wake (as indicated by the turbulence intensity in Fig. 11) has not yet penetrated the wall region. The data at 50% chord indicate considerable spreading of the wake (Figs 4, 5, and 9–11). With fully developed turbulent flow in the wake region (trajectory W), the width of the turbulent region reaches a maximum value near the wall and decreases rapidly to zero near the outer layer. Even here the maximum turbulent kinetic energy region has not been able to penetrate the wall region, and the calm region is sandwiched between this spot and the wall (Figs. 9 and 11). At the 70% chord, the wake has spread out considerably, diffusing the turbulence in the lateral and the normal directions; peak turbulent kinetic energy is confined to a very small region during the wake-passing period. The calm region appears in the trailing regions of the wake, indicated by lower values of C_f. At the 90% chord, the wake occupies most of the period and the calm region is confined to a small region

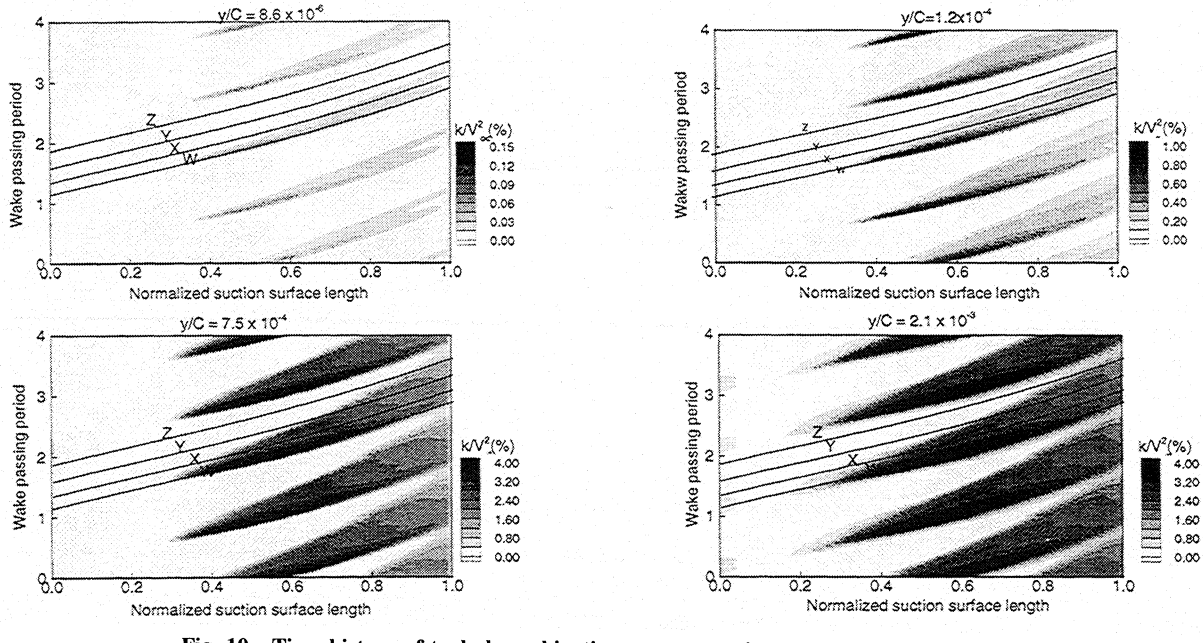

Fig. 10 Time history of turbulence kinetic energy at various distances from the wall.

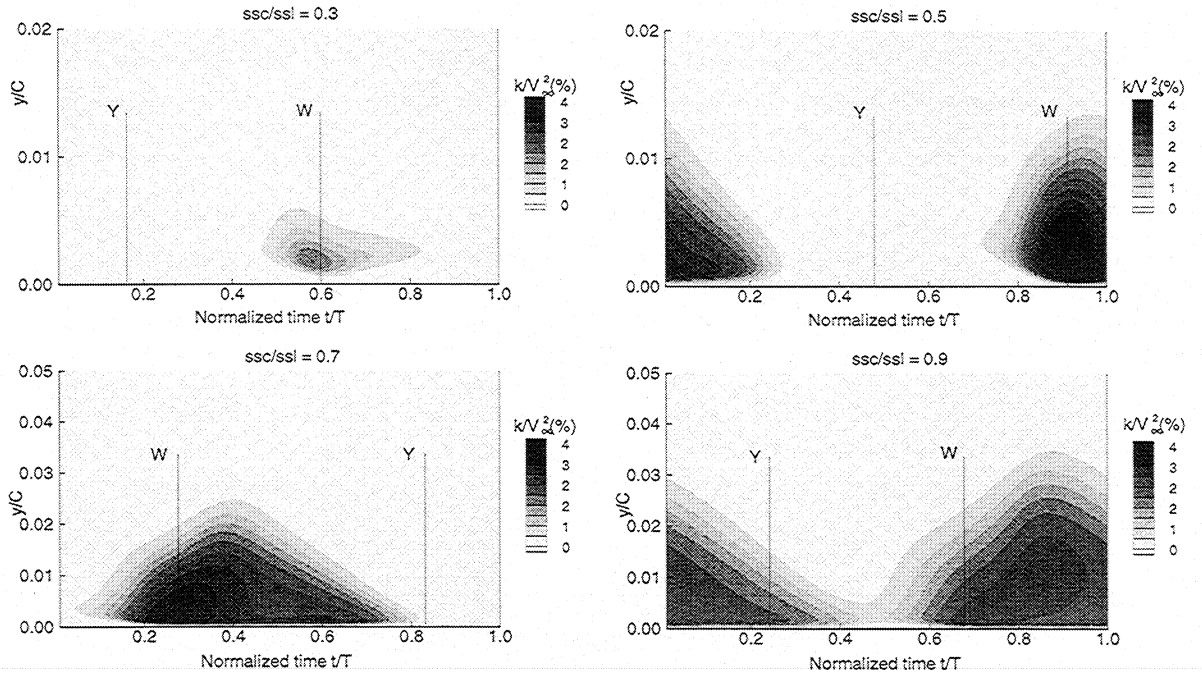

Fig. 11 Time history of turbulent kinetic energy in one period.

beneath the wake near the trailing edge (Figs. 9 and 11, $t/T \approx 0.5$). The maximum turbulent kinetic energy has decreased from its upstream value. The flow is fully turbulent and the momentum thickness distribution (Fig. 5) follows very closely the distribution of turbulence intensity (Fig. 11). It should be noted that the boundary momentum thickness is the lowest from $t/T = 0.4$–0.6 (Fig. 5), which is consistent with the height of turbulent kinetic energy (maximum to freestream value) intensity profiles shown in Fig. 11.

The present Navier–Stokes solution follows the general features of the experiment better than the Euler/boundary-layer solution. The Euler/boundary-layer solution is much more diffusive. Thus, the Navier–Stokes procedure shows considerable promise in capturing the flow physics associated with the rotor–stator interaction, provided the turbulence amplification/modification near the leading edge is captured accurately.

Concluding Remarks

A Navier–Stokes code was used to simulate the unsteady transitional boundary layer caused by rotor–stator interaction. Three low Reynolds turbulence models and two modifications to reduce the excessive generation of turbulent kinetic energy near the leading edge were tested. The present numerical solution was validated with the experimental data and the computational result obtained by using the boundary-layer computation coupled with the unsteady Euler solution.

Among the three low-Reynolds turbulence models tested in this paper, Fan et al.'s[6] turbulence model was the best in terms of numerical stability and predictability of the wake-induced transition strip. Launder's[15] modification to reduce the excessive generation of turbulent kinetic energy near the leading edge worked better than Strahle's modification. The present Navier–Stokes solution with Fan et al.'s model modified with Launder's suggestion showed the best accuracy. But Launder's modification is still not satisfactory and requires further research to capture the flow physics associated with transitional flows in turbomachinery. The laminar boundary layer near the leading edge and the calmed region was not captured well.

The present approach shows good qualitative agreement with the experiment and showed a better prediction for the onset of transition and its length than the boundary-layer approach coupled with the unsteady Euler solution. The wake-induced transitional strip and the unsteadiness caused by the upstream wake were also well captured. The unsteady transition is triggered as the rotor wake develops into unsteady vortices after impinging on the blade surface. The region of high turbulence kinetic energy coincides with the region of strong unsteady velocity vector and vorticity.

Acknowledgments

This work was partially supported by the Korea Science and Engineering Foundation through a postdoctoral fellowship for the senior author; and partially funded through the Office of Naval Research, Contract N00014-90-J1182, with J. Fein as the Contact Monitor. The authors acknowledge the availability of computer resources at the Pittsburgh Super Computer Center and the National Aerospace Simulation facility at the NASA Ames Research Center. The authors also acknowledge D. Wisler and D. Halstead for providing experimental data, and W.-S. Yu for assistance with computations.

References

[1]Fan, S., and Lakshminarayana, B., "Computation and Simulation of Wake-Generated Unsteady Pressure and Boundary Layers in Cascades," *Journal of Turbomachinery*, Vol. 118, No. 1, 1996, pp. 96–122.

[2]Schulze, H. D., Gallus, H. E., and Lakshminarayana, B., "Three Dimensional Separated Flow Field in the End Wall Region of an Annular Compressor Cascade in the Presence of Rotor-Stator Interaction," *Journal of Turbomachinery,* Vol. 112, 1990, pp. 669–690.

[3]Halstead, D. E., Wisler, D. C., Okiishi, T. H., Walker, G. J., Hodson, H. P., and Shin H.-W., "Boundary Layer Development in Axial Compressors and Turbines," Part 1: Composite Picture, Part 2: Compressors, Part 3: LP Turbines, Part 4: Computations and Analysis, American Society of Mechanical Engineers, Papers 95-GT-461, 462, 464, New York, 1995.

[4]Chien, K. Y., "Prediction of Channel and Boundary Layer Flows with a Low Reynolds Number Turbulence Model," *AIAA Journal*, Vol. 20, 1982, pp. 33–38.

[5]Lam, C. K. G., and Bremhost, K., "A Modified Form of the k-ε Model for Predicting Wall Turbulence," *Journal of Fluids Engineering*, Vol. 103, 1981, pp. 456–460.

[6]Fan, S., Lakshminarayana, B., and Barnett, M., "A Low Reynolds Number k-ε Model for Unsteady Turbulent Boundary Layer Flows," *AIAA Journal*, Vol. 31, No. 10, 1993, pp. 1777–1784.

[7]Chakka, P., and Schobeiri, M. T., "Modeling Unsteady Boundary Layer Transition on a Curved Plate Under Periodic Unsteady Flow Conditions: Aerodynamic and Heat Transfer Investigations," American So-

ciety of Mechanical Engineers, Paper 97-GT-399, New York, 1997.

[8]Abu-Ghannam, B. J., and Shaw, R., "Natural Transition of Boundary Layers—The Effect of Turbulence, Pressure Gradient and Flow History," *Journal of Mechanical Engineering Sciences*, Vol. 22, 1980, pp. 213–228.

[9]Savill, A. M., "On Point Closure Applied to Transition," *Turbulence and Transition Modelling*, Kluwer Academic, Norwell, MA, 1995, pp. 233–265.

[10]Ho, Y. H., and Lakshminarayana, B., "Computation of Unsteady Viscous Flow Using an Efficient Algorithm," *AIAA Journal*, Vol. 31, No. 12, 1993, pp. 2232–2241.

[11]Stauter, R. C., Dring, R. P., and Carta, F. O., "Temporally and Spatially Resolved Flow in a Two-Stage Axial Compressor, Part 1: Experiment," American Society of Mechanical Engineers, Paper 90-GT-259, New York, 1990.

[12]Gundy-Burlet, K. L., Rai, M. M., Stauter, R. C., and Dring, R. P., "Temporally and Spatially Resolved Flow in a Two-Stage Axial Compressor, Part 2: Computational Assessment," American Society of Mechanical Engineers, Paper 90-GT-299, New York, 1990.

[13]Kunz, R., and Lakshminarayana, B., "Explicit Navier-Stokes Computation of Cascade Flow Using the k-ε Turbulence Model," *AIAA Journal*, Vol. 30, No. 1, 1992, pp. 13–22.

[14]Power, G. D., Verdon, J. M., and Kousen, K. A, "Analysis of Unsteady Compressible Viscous Layers," *Journal of Turbomachinery*, Vol. 133, No. 4, 1991, pp. 644–653.

[15]Launder, B. E., "Modeling Convective Heat Transfer in Complex Turbulent Flows," *Engineering Turbulence Modeling and Experiments 2*, Elsevier, Amsterdam, 1993, pp. 3–22.

[16]Strahle, W. C., "Stagnation Point Flows with Free-stream Turbulence—The Matching Condition," *AIAA Journal*, Vol. 23, No. 11, 1985, pp. 1822–1824.

[17]Zerkle, R. D., and Lounsbury, R. J., "The Influence of Freestream Turbulence and Pressure Gradients on Heat Transfer by Turbine Airfoils," AIAA Paper 87-1917, 1987.

[18]Jennions, I. K., and Turner, M. G., "Three-Dimensional Navier-Stokes Computations of Transonic Fan Flow Using an Explicit Flow Solver and an Implicit k-ε Solver," *Journal of Turbomachinery*, Vol. 115, 1987, pp. 261–272.